The 2009 IEEE/RSJ International Conference on
Intelligent Robots and Systems
October 11-15, 2009 St. Louis, USA

Kinematic Analysis and Design of a New 3T1R 4-DOF Parallel Mechanism with Rotational Pitch Motion

Sung Mok Kim, Wheekuk Kim, and Byung-Ju Yi

Abstract— **Less degree-of-freedom robots are useful for special applications. Specifically, practical application of 4-DOF parallel mechanism has been rare, though synthesis on this type has been conducted quite a few. Recently, we proposed a revolute joint-based 3T1R 4-DOF parallel mechanism having Schonflies motions whose output rotational motion is a roll motion. This work proposes another type of a new 3T1R 4-DOF parallel mechanism having Schonflies motions whose rotational motion is a pitch motion. The position analysis and kinematic modeling for the mechanism are performed, and its workspace size and kinematic characteristic with respect to the kinematic isotropic characteristic are examined. To support high potential of the mechanism for real applications, three different versions are suggested and each motion capability is verified through its simulator. Finally, a prototype is developed to verity its actual motion capability.**

I. Introduction

PARALLEL structure is known to have high rigidity, high precision, and improved dynamic characteristic which could be obtained by placing heavy actuators toward the ground. Due to those useful advantages of parallel structure over serial structure, a variety of parallel mechanisms has been proposed and investigated so far. [1][2]

In the past decade, there has been a quite amount of studies on structural synthesis conducted to identify feasible structure for parallel mechanisms having 4 degrees of freedom or 5 degrees of freedom. Huang and Li [3] conducted type synthesis of symmetrical lower degree-of-freedom parallel mechanism using the constraint synthesis method and proposed several 4-DOF parallel mechanisms such as 3R1T, 2R2T, and 3T1R types. Fang and Tsai [4] proposed a systematic method for the structural synthesis of a class of 4-DOF and 5-DOF parallel mechanisms with identical sub-chains. Kong and Gosselin [5] investigated type synthesis of 4-DOF parallel mechanisms with Schonflies motions based on screw theory and suggested several parallel mechanisms with identical four chains. Gao, et al. [6] suggested several types of composite pairs and new limbs with specific degrees of freedom and suggested several new types of less degree-of-freedom parallel mechanisms. Zlatanov and Gosselin[7][8] investigated singularity of a family of 3R1T parallel mechanisms and suggested a number of new 4-DOF SP-equivalent parallel mechanisms through type synthesis. So far, most of those works have focused on fully parallel structure with simple pair of joints and however, practical applications of 4-DOF parallel mechanisms reported are limited and further investigation is necessary.

Particularly, the 4-DOF parallel mechanisms having Schonflies motions (or SCARA motions) could be useful in industrial operations such as assembly, riveting, screwing and pick-and-place tasks. Clavel [9] introduced a very nice design (it is called Delta robot) using planar parallelograms which is only based on revolute joint and very effective for high speed industrial assembly applications. Since then, there have been several other practical 3T1R type parallel mechanisms with identical four chains suggested by Company et al. and Salgado et al [10]-[14]. Gogu[15] focused on fully-isotropic property of parallel mechanisms by conducting structural synthesis and suggested several fully-isotropic parallel robots with Schonflies motions. Recently, Kim et al [16] suggested a revolute-joint-based 4-DOF parallel mechanism with Schonflies motions(three translational motions and one rotational roll motion of the moving platform). In their work, asymmetric assignment of offset angles on the moving plate of the mechanism was suggested to remove architectural singularity from useful workspace.

In this work, another type of 3T1R 4-DOF mechanism having Schonflies motions (i.e., 3-DOF translational motion and one rotational pitch motion) is investigated. Section II describes the structure of this mechanism. The kinematic analysis is conducted in section III. In section IV, workspace and isotropic characteristic of the proposed mechanism are investigated. In section V, three different versions are suggested and a prototype mechanism is developed to show its motion capability. Conclusion is drawn in section VI.

II. Concept of The Proposed 4-DOF Mechanism

Figure 1 shows the proposed mechanism. The mechanism has four hybrid sub-chains and geometric structure of each hybrid sub-chain is almost identical to that of Delta robot [9]. However, at the ends of two hybrid sub-chains which are connected to the moving plate (shown as a cross-shaped body in the figure), two additional revolute joints are placed to allow the rotational pitch motion of the moving plate.

Wheekuk Kim and Sung Mok Kim are with Department of Control and Instrumentation Engineering, Korea University, Korea. (corresponding author phone +82-41-860-1443; fax: +82-41-865-1820; e-mail: wheekuk@korea.ac.kr).

Byung-Ju Yi with School of Electrical Engineering and Computer Science, Hanyang University, Korea (e-mail: bj@hanyang.ac.kr).

With this arrangement, the proposed mechanism turns out to have 4-DOF Schonflies motions; 3-DOF translational motion and one rotational motion about the axis along which those two added revolute joint axes are aligned.

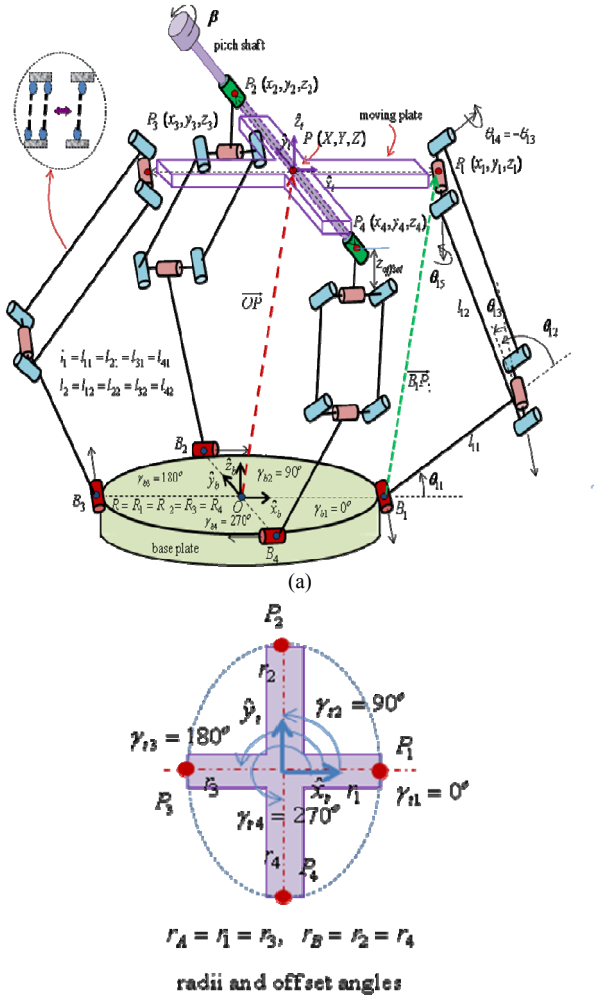

(a)

(b)

Fig. 1. (a) The proposed 4-DOF mechanism. (b) Radii and offset angles on the moving plate.

Note that as can be seen in Fig. 1, the proposed mechanism has a structure such that the rotational pitch motion is controlled by two hybrid sub-chains while the other two hybrid sub-chains support the pitch axis. This structure allows more design flexibility to convert the rotational pitch motion into the other types of rotational motion (i.e., either roll motion or yaw motion) or to attach a transmission device to magnify the pitch motion range. Two other different designs utilizing this feature are suggested later in this paper. Also, it can be noted that friction and the dynamic inertial load would be minimal since this mechanism only uses revolute joints and all of four actuators could be placed on the base platform. Thus, this system would be expected to have very high potential to various applications.

III. Kinematic Analysis

A. Inverse Position Analysis

In this section, the inverse position analysis of the parallel mechanism model shown in Fig. 1 is performed. The origin of the base frame $(\hat{x}_b, \hat{y}_b, \hat{z}_b)$ and the output frame $(\hat{x}_t, \hat{y}_t, \hat{z}_t)$ of the mechanism is defined at the center of the base plate and at the center of the moving plate, respectively. The first joint of each of four legs $(i = 1, 2, 3, 4)$ is located on the base plate on a circle of radius R with an offset angle γ_{bi} from the $\hat{x}_b$ axis, respectively. Similarly, the contact point of each of four legs with the moving plate is placed with distance r_i from the center of the moving plate and with an offset angle γ_{ti} from $\hat{x}_t$ axis, respectively. θ_{ij} and l_{ij} denote the j^{th} joint of the i^{th} subchain and the j^{th} link length of the i^{th} subchain of the mechanism, respectively.

In Fig. 1, the position vector $\overrightarrow{B_iP_i}$ from B_i to P_i in the base frame can be written as

$$\overrightarrow{B_iP_i} = \overrightarrow{OP} + \overrightarrow{PP_i} - \overrightarrow{OB_i} = \overrightarrow{OP_i} - \overrightarrow{OB_i}, \quad for\ i = 1,2,3,4 \quad (1)$$

where $\overrightarrow{OP}$ representing the absolute position vector from the origin of the base frame to the origin of the output frame and $\overrightarrow{OB_i}$ representing the absolute position vector from the base origin to the first joint of the i^{th} subchain can be expressed, respectively, as

$$\overrightarrow{OP} = (X, Y, Z)^T, \quad (2)$$

$$\overrightarrow{OB_i} = (Rc\gamma_{bi}, Rs\gamma_{bi}, 0)^T. \quad (3)$$

And $\overrightarrow{PP_i}$ denoting the absolute position vector from the origin of the output frame to the last joint of the i^{th} sub-chain can be expressed as

$$\overrightarrow{PP_i} = Rot(\hat{y}, \beta)Rot(\hat{z}, \gamma_{ti})\begin{Bmatrix} r_i \\ 0 \\ 0 \end{Bmatrix} = \begin{Bmatrix} r_i c\beta s\gamma_{ti} \\ r_i s\gamma_{t2} \\ -r_i c\beta c\gamma_{ti} \end{Bmatrix}, \ for\ i = 1,3, \quad (4)$$

and

$$\overrightarrow{PP_i} = \mathrm{Rot}(\hat{z}, \gamma_{ti})\begin{Bmatrix} r_i \\ 0 \\ 0 \end{Bmatrix} + \begin{Bmatrix} 0 \\ 0 \\ -z_{offset} \end{Bmatrix} = \begin{Bmatrix} r_i c\gamma_{ti} \\ r_i s\gamma_{ti} \\ -z_{offset} \end{Bmatrix} \quad for\ i = 2,4, \quad (5)$$

where z_{offset} denotes offset distance from the point (either P_2 or P_4) to the pitch joint axis along the $\hat{z}_t$ direction. The position vector $\overrightarrow{B_iP_i} = (x_i', y_i', z_i')^T$ represented in the base frame in terms of joint displacement variables can be expressed as

$$x_i' = c\gamma_{bi}(l_{i2}c\theta_{i12}c\theta_{i3} + l_{i1}c\theta_{i1}) + l_{i2}s\gamma_{bi}s\theta_{i3}, \quad (6)$$

$$y_i' = s\gamma_{bi}(+l_{i2}c\theta_{i12}c\theta_{i3} + l_{i1}\,\mathrm{c}\,\theta_{i1}) - l_{i2}c\gamma_{bi}s\theta_{i3}, \quad (7)$$

$$z_i' = l_{i2}s\theta_{i12}c\theta_{i3} + l_{i1}s\theta_{i1}, \quad (8)$$

where $c\theta_{i1} = cos\theta_{i1}$, $s\theta_{i1} = sin\theta_{i1}$, $c\theta_{i12} = cos(\theta_{i1} + \theta_{i2})$, and $s\theta_{i12} = sin(\theta_{i1} + \theta_{i2})$ are used for simplicity.

As the output vector of the mechanism, the center position (X, Y, and Z) and the rotational angle β about the $\hat{y}_t$ axis of the moving plate are selected. Thus, in the inverse position analysis, all the joint angles of the parallel mechanism need to be found when those four output variables are given. Now, the process of finding the joint angles of the hybrid chain will be discussed. Noting that the absolute position vector $\overrightarrow{B_iP_i}$ can be expressed in local frame of the corresponding sub-chain as

$$\overrightarrow{B_iP_i}^{(i)} = [{}^b_t R]^T \overrightarrow{B_iP_i} \tag{9}$$

where

$$\overrightarrow{B_iP_i}^{(i)} = (x'_{(i)}, y'_{(i)}, z'_{(i)})^T, \tag{10}$$

$$[{}^b_t R] = Rot(\hat{z}, \gamma_{bi}) rot(\hat{x}, 90^o) = \begin{bmatrix} c\gamma_{bi} & 0 & s\gamma_{bi} \\ s\gamma_{bi} & 0 & -c\gamma_{bi} \\ 0 & 1 & 0 \end{bmatrix}, \tag{11}$$

(1) can be rewritten as follows:

$$\overrightarrow{B_iP_i}^{(i)} = [{}^b_t R]^T (\overrightarrow{OP_i} - \overrightarrow{OB_i}), \ for\ i = 1,2,3,4. \tag{11}$$

LHS of (11) can be found from (6)-(9) as

$$x'_{(i)} = l_{i2} c\theta_{i12} c\theta_{i3} + l_{i1} c\theta_{i1}, \tag{12}$$

$$y'_{(i)} = l_{i2} s\theta_{i12} c\theta_{i3} + l_{i1} s\theta_{i1} \tag{13}$$

$$z'_{(i)} = l_{i2} s\theta_{i3}, \tag{14}$$

and RHS of (11) can be found from (2)-(5) as

$$\begin{Bmatrix} x'_{(i)} \\ y'_{(i)} \\ z'_{(i)} \end{Bmatrix} = \begin{Bmatrix} c\gamma_{bi}(X + r_i c\beta s\gamma_{bi} - Rc\gamma_{bi}) + s\gamma_{bi}(Y + r_i s\gamma_{ti} - Rs\gamma_{bi}) \\ Z - r_i c\beta c\gamma_{ti} \\ s\gamma_{bi}(X + r_i c\beta s\gamma_{bi} - Rc\gamma_{bi}) - c\gamma_{bi}(Y + r_i s\gamma_{ti} - Rs\gamma_{bi}) \end{Bmatrix} \quad for\ i = 1,3, \tag{15}$$

$$\begin{Bmatrix} x'_{(i)} \\ y'_{(i)} \\ z'_{(i)} \end{Bmatrix} = \begin{Bmatrix} c\gamma_{bi}(X + r_i c\gamma_{bi} - Rc\gamma_{bi}) + s\gamma_{bi}(Y + r_i s\gamma_{ti} - Rs\gamma_{bi}) \\ Z - z_{offet} \\ s\gamma_{bi}(X + r_i s\gamma_{bi} - Rc\gamma_{bi}) - c\gamma_{bi}(Y + r_i s\gamma_{ti} - Rs\gamma_{bi}) \end{Bmatrix} \quad for\ i = 2,4. \tag{16}$$

Now, (11) is rearranged as follows

$$x'_{(i)} - l_{i1} c\theta_{i1} = l_{i2} c\theta_{i12} c\theta_{i3}, \tag{17}$$

$$y'_{(i)} - l_{i1} s\theta_{i1} = l_{i2} s\theta_{i12} c\theta_{i3}, \tag{18}$$

$$z'_{(i)} = l_{i2} c\theta_{i3}. \tag{19}$$

Squaring these three equations and adding them altogether yields the following form

$$A_i c\theta_{i1} + B_i s\theta_{i1} = C_i, \tag{20}$$

where

$$A_i = 2x'_{(i)} l_{i1}, \tag{21}$$

$$B_i = 2y'_{(i)} l_{i1}, \tag{22}$$

$$C_i = l_{i1}^2 + x'^{\,2}_{(i)} + y'^{\,2}_{(i)} + z'^{2}_{(i)} - l_{i2}^2. \tag{23}$$

Using the tangent half angle substitutions, θ_{i1} can be found from Eq. (12) as

$$\theta_{i1} = Atan2(B_i, A_i) \pm Atan2(\sqrt{A_i^2 + B_i^2 - C_i^2}, C_i). \tag{24}$$

By squaring (17) and (18) and adding them results in

$$\theta_{i3} = \pm\sqrt{(x'_{(i)} - l_{i1} c\theta_{i1})^2 + (y'_{(i)} - l_{i1} s\theta_{i1})^2} / l_{i2}. \tag{25}$$

To find θ_{i1}, we substitute (20) and (25) into (17) and (18) to find

$$(l_{i2} c\theta_{i3} c\theta_{i1}) c\theta_{i2} - (l_{i2} c\theta_{i3} s\theta_{i1}) s\theta_{i2} = x'_{(i)} - l_{i1} c\theta_{i1} \tag{26}$$

$$(l_{i2} c\theta_{i3} s\theta_{i1}) c\theta_{i2} + (l_{i2} c\theta_{i3} c\theta_{i1}) s\theta_{i2} = y'_{(i)} - l_{i1} s\theta_{i1}. \tag{27}$$

Applying Cramer's rule to (26) and (27), θ_{i2} can be found as

$$\theta_{i2} = atan2(s\theta_{i2}, c\theta_{i2}). \tag{28}$$

For θ_{14}, it is obvious that

$$\theta_{14} = -\theta_{13}, \tag{29}$$

since the parallelogram four-bar chain is constrained to satisfy this condition. Noting that the top plate has only one-DOF rotational motion about the $\hat{y}_t$ axis, θ_{i5} can be computed as

$$\theta_{i5} = \beta - \theta_{i1} - \theta_{i2}, \ for\ i = 1,3. \tag{30}$$

$$\theta_{i5} = -\theta_{i1} - \theta_{i2}, \ for\ i = 2,4. \tag{31}$$

B. Forward Position Analysis

In this section, we describe the forward position analysis of the parallel model given in Fig. 1. Consider the case that we have only four base joint angles $(\theta_{11}, \theta_{21}, \theta_{31}, \theta_{41})$ measured and want to find output position and orientation, (namely, X, Y, Z and β). Eq. (20) represents four inverse position equations when x_i, y_i, z_i are replaced by X, Y, Z and β as shown in Eqs. (15) and (16). Numerical methods can be employed to find the forward position solution.

C. First-order Kinematics

The first-order kinematics relates the output velocity vector to the input joint velocity vector. The velocity relation between the output vector of the parallel manipulator and joint vector for the i^{th} subchain can be found as

$$\dot{\boldsymbol{u}} = \left[{}_i G^u_\theta \right] {}_i\dot{\boldsymbol{\theta}} \tag{32}$$

by direct differentiation of Eqs. (11) and (30) with respect to time. In Eq. (32),

$$\dot{\boldsymbol{u}} = \left[\dot{X}, \dot{Y}, \dot{Z}, \dot{\beta} \right]^T, \tag{33}$$

$${}_i\dot{\boldsymbol{\theta}} = \left[\dot{\theta}_{i1}, \dot{\theta}_{i2}, \dot{\theta}_{i3}, \dot{\theta}_{i5} \right]^T, \ for\ i = 1,3 \tag{34}$$

$${}_i\dot{\boldsymbol{\theta}} = \left[\dot{\theta}_{i1}, \dot{\theta}_{i2}, \dot{\theta}_{i3}, \dot{\theta}_{i6} \right]^T, \ for\ i = 2,4. \tag{35}$$

Note that $\dot{\theta}_{i6} = \dot{\beta}$. Now, the inverse relation for each serial subchain of the manipulator can be written as

$${}_i\dot{\boldsymbol{\theta}} = \left[{}_i G^u_\theta \right]^{-1} \dot{\boldsymbol{u}}, \ for\ i = 1,2,3,4. \tag{36}$$

where it is assumed that the Jacobian $[{}_i G^u_\theta]$ is invertible. Considering the four base joints of the parallel manipulator as the active joints where actuators are placed, the velocity

relation relating the output vector to the active joint vector can be constructed by selecting the first row of each inverse-Jacobian of the four serial subchains and forming a matrix relation as below

$$\dot{\boldsymbol{\theta}}_{\boldsymbol{a}} = \left[G_u^a \right] \dot{\boldsymbol{u}}, \tag{37}$$

where

$$\left[G_u^a \right] = \begin{bmatrix} \left[{}_1G_\theta^u \right]^{-1}_{(1;*)} \\ \left[{}_2G_\theta^u \right]^{-1}_{(1;*)} \\ \left[{}_3G_\theta^u \right]^{-1}_{(1;*)} \\ \left[{}_4G_\theta^u \right]^{-1}_{(1;*)} \end{bmatrix}, \tag{38}$$

$$\dot{\boldsymbol{\theta}}_{\boldsymbol{a}} = \left[\dot{\theta}_{11}, \dot{\theta}_{21}, \dot{\theta}_{31}, \dot{\theta}_{41} \right]^T, \tag{39}$$

and $[G_\theta^u]_{(i,*)}$ denotes the i^{th} row vector of $[G_\theta^u]$. Now, inverting the relation of Eq. (37) yields a first-order forward kinematics relation of the system, given as

$$\dot{\boldsymbol{u}} = \left[G_a^u \right] \dot{\boldsymbol{\theta}}_{\boldsymbol{a}}, \tag{40}$$

where

$$\left[G_a^u \right] = \left[G_u^a \right]^{-1}. \tag{41}$$

IV. Kinematic Design and Characteristic

A. Kinematic Design Indices

Two design aspects are considered: workspace size and kinematic isotropic property of the mechanism. The kinematic isotropic property can be examined via kinematic isotropic index σ_I which is defined as

$$\sigma_I = \frac{\sigma_{\min}}{\sigma_{\max}}, \tag{42}$$

where $\sigma_{\min}$ and $\sigma_{\max}$ denote the minimum and maximum singular value of $[G_a^{u^*}]$, respectively. Noting that the proposed mechanism has 3-DOF translational motions and 1-DOF rotational motion, there exists dimensional difference of the two different motion spaces. There have been several approaches suggested to handle this matter [17][18]. However, for our simplicity, we select a nominal ratio of the angularity velocity to the translational velocity as $v_{max} : \dot{\beta}_{max} = 1 : 1/r_A$ such that the magnitude of the translational velocity at the point P_i ($for\ i = 1\ or\ 3$) caused by the pure pitch angular velocity to be equal to the one caused by the pure translational velocity of the moving plate along the same direction, where it is assumed that $r_A = r_1 = r_3$ for simplicity. Thus, we normalize the Jacobian elements as follows:

$$\dot{\boldsymbol{u}}^* = \begin{Bmatrix} \dfrac{v}{v_{max}} \\ \dfrac{\dot{\beta}}{\dot{\beta}_{max}} \end{Bmatrix} = \begin{bmatrix} \dfrac{[I]_{3x3}}{v_{max}} & [0]_{3x1} \\ [0]_{1x3} & \dfrac{1}{\dot{\beta}_{max}} \end{bmatrix} \left[G_a^u \right] \dot{\boldsymbol{\theta}}_{\boldsymbol{a}} = \left[G_a^{u^*} \right] \dot{\boldsymbol{\theta}}_{\boldsymbol{a}}. \tag{43}$$

The workspace of manipulator can be found as

$$W = \int_w dw. \tag{44}$$

However, noting that the size and shape of the dexterous workspace of the mechanism is so complex due to singularities within workspace, approximate workspace plots are obtained by defining an appropriate threshold value of kinematic isotropic index instead of computing the workspace as in (44).

B. Kinematic Design

In fact, there are many design parameters of the proposed mechanism to consider such as γ_{bi}, γ_{ti}, R, r_i, l_{i1}, l_{i2} and z_{offset} for $i = 1, 2, 3, 4$ as shown in Fig. 1. Numerous trial simulations have been conducted to search sub-optimal design parameters which could secure both large singularity-free workspace and better kinematic isotropic property within the workspace. In this process, we tried to give favor to symmetric design parameters unless they create architectural singularity within center area of workspace as addressed in [16] and do not cause mechanical interferences. And some of optimal kinematic design results from [16] are adapted.

The radii of the locations of revolute joints on the base and on the moving plate, and link lengths of the lower and upper links are set, respectively, as $R = 50mm$, $r_A = r_1 = r_2 = 20mm$, $r_B = r_2 = r_4 = 30mm$ and $l = l_{i1} = l_{i2} = 75mm$. Also, offset angles on the base and on the moving plate are selected symmetrically distributed as $\gamma_{bi} = 0^o, 90^o, 180^o, 270^o$, and $\gamma_{ti} = 0^o, 90^o, 180^o, 270^o$, respectively. And lastly, the offset distance from the points P_2 and P_4 on the moving plate to the pitch joint axis along the $\hat{z}_t$ direction is set as $z_{offset} = 0mm$.

Now, we would like to assess the characteristic of the mechanism with those design parameters. Figure 2 shows the sets of translational workspace plots in the $x-y$ plane for the mechanism for different values of $Z = 20mm, 40mm, 60mm, 80mm, 100mm, 120mm$ when $\beta = 30^o, 60^o, 90^o, 120^o, 150^o$, respectively. In this simulations, the search ranges for x, y and z coordinates are set as $-100mm \le X, Y \le 100mm$ and $20mm \le Z \le 120mm$, and the one for the rotational output angle β is set as $30^o \le \beta \le 150^o$ noting that when either $\beta = 0^o$ or $\beta = \pm 180^o$, i.e. the moving plate is parallel to the base plate, the mechanism becomes singular. And the grid interval in the $x-y$ plane is set as $0.25mm$.

In Fig. 2, the workspace boundary was identified as the region in which the local kinematic isotropic index value is greater than a predefined threshold value (0.005). With this

threshold value, accurate trajectories of all singular configurations could be effectively shown as in figures. In fact, there exist several singular configuration trajectories making the region of the workspace close to the base plate not useful. However, it can be noted from these plots that acceptable size/**s**hape of singularity-free workspace exists around the middle region of the workspace.

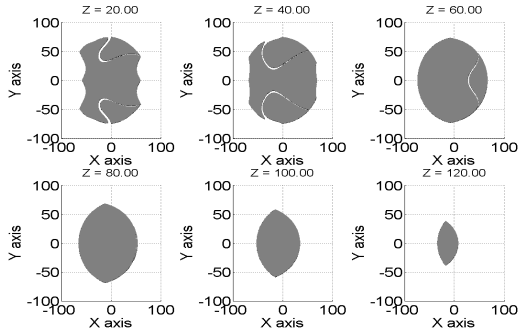

(a)

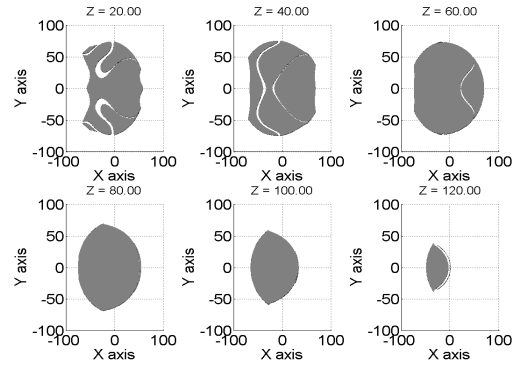

(b)

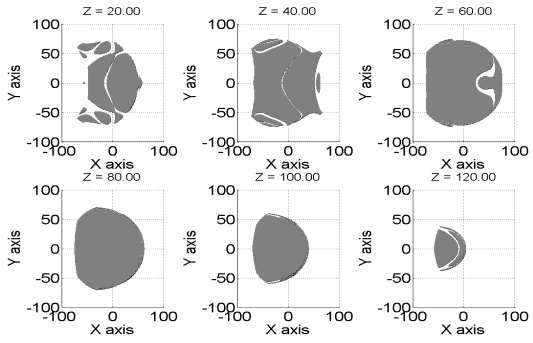

(c)

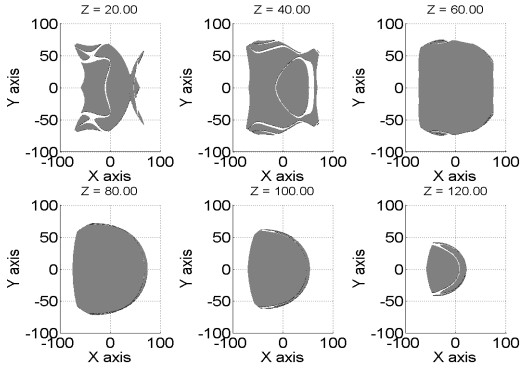

(d)

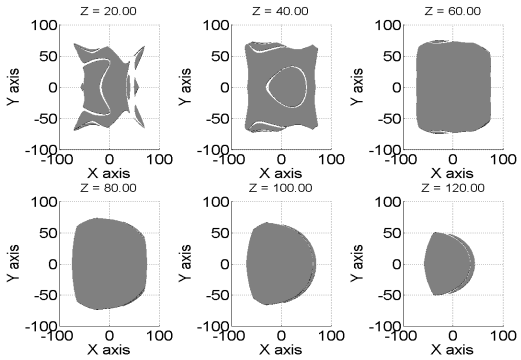

(e)

Fig. 2. Workspace on the $x-y-z$ domain. (a) $\beta = 30^{o}$. (b) $\beta = 60^{o}$. (c) $\beta = 90^{o}$. (d) $\beta = 120^{o}$. (e) $\beta = 150^{o}$.

Figure 3 shows isotropic index plots in the x-y plane for different values of $Z = 60mm, 80mm, 100mm$, respectively, for a fixed $\beta = 90^{o}$. Though not enough plots are shown about isotropic property of the mechanism here, it is observed that the proposed mechanism has acceptable kinematic isotropic characteristics around the middle of workspace for practical applications. With an optimal kinematic design as in [14], better characteristics of the mechanism could be secured. In the following section, three practical modified designs for the proposed mechanism are discussed.

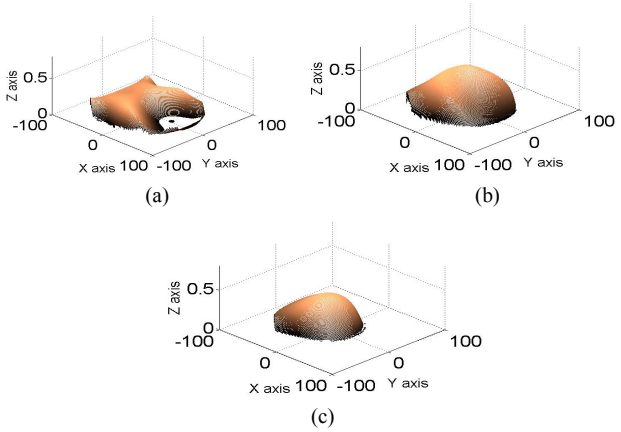

(a) (b)

(c)

Fig. 3. Isotropic index plots in the x-y plane for a fixed $\beta = 90^{o}$. (a) $z = 60mm$. (b) $z = 80mm$. (c) $z = 100mm$.

V. Implementation

Three different versions for the proposed parallel mechanism are considered. Figure 4a) shows the first version whose output plate is attached at one end of the pitch shaft. This version could be employed as an assembly robot to conduct tasks requiring inserting parts into holes with desired orientations or as a haptic device. Figure 4b) shows the second version. In this version, the pitch motion is switched into the roll motion through gear trains attached. This version could be employed as a robot conducting screwing tasks, part assembly tasks requiring the orientation

control or as a haptic device. Figure 4c) shows the last version of the mechanism. In this version, the pitch axis lies on the cross-shaped moving plate and an output plate is attached above the moving plate with an offset distance to avoid mechanical interference with the hybrid chains which move close to the center of the cross-shaped top plate as shown in the figure.

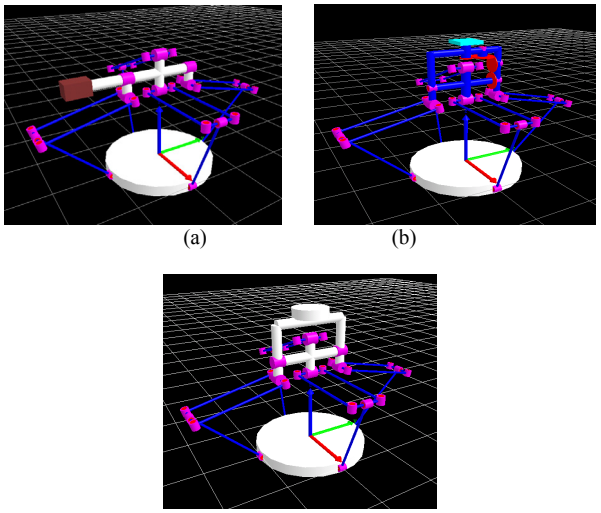

(a) (b) (c)

Fig. 4. Three different versions of the proposed mechanism. (a) The first version . (b) The second version. (c) The third version.

The first version of the proposed 4-DOF parallel mechanism was implemented and its motion capability was tested. Fig. 5 shows the prototype of this mechanism. The attached video clip demonstrates simulated motions of three different versions as well as the actual motion of the implemented mechanism.

(a) (b)

Fig. 5. Prototype and its 4-DOF motions. (a) Translation. (b) Rotation.

VI. Conclusions

In this work, we proposed a new parallel manipulator with Schonflies motions (three translational degrees of freedom and one rotational degree of freedom about the pitch axis). Secondly, its position analysis and first-order kinematic analysis are performed. Then through the investigation on workspace shape and size along with its local kinematic isotropic property, the potential of the proposed mechanism in aspects of real applications is shown. Further, three different designs of the proposed mechanism are suggested and each motion capability is verified through simulations. Currently, the singularity analysis of the proposed mechanism is ongoing and as the future work, we plan to conduct optimization of these three different designs to secure both larger singularity-free, dexterous workspace and improved kinematic characteristic, and use them as haptic devices or other applications such as assembling, screwing or bolting robots by attaching it to the end of a large sized manipulator.

References

[1] J.P. Merlet, *Parallel Robots*, Kluwer Academic Publishers, 2000.

[2] L.-W. Tsai, *Robot Analysis: the mechanics of serial and parallel manipulators*, Wiley Interscience, 1999.

[3] Z. Huang and Q. C. Li, "Type synthesis of symmetrical lower-mobility parallel mechanism using the constraint-synthesis method," *Int. J. Robot. Res*., vol. 22, no. 1, pp. 59–79, Jan, 2003

[4] Y. Fang and L.-W. Tsai, "Structure synthesis of a class of 4-DOF and 5-DOF parallel manipulators with identical limb structures," *Int. J. Robot. Res*., vol. 21, no. 9, pp. 799–810, Sep, 2002.

[5] X. Kong and C.M. Gosselin, "Type synthesis of 3T1R 4-DOF parallel manipulators based on screw theory," *IEEE Trans. Robot. Auto*., vol. 20, no. 2, pp. 181–190, Apr. 2004.

[6] F. Gao, W. Li, X. Zhao, A. Jin, and H. Zhao, "New kinematic structures for 2-, 3-, 4-, and 5-DOF parallel manipulator designs," *Mech. Mach. Theory*, vol. 37, 2002, 1395-1411.

[7] D. Zlatanov, M. Zoppi and C.M. Gosselin, "Singularities and mobility of a class of 4-DOF mechanisms," *On advances in robot kinematics*, Kluwer Academic Publishers, pp. 105-112, 2004.

[8] X. Kong and C.M. Gosselin, "Type synthesis of 4-DOF SP-equivalent parallel manipulators: a virtual chain approach," *Mechanism and machine theory*, vol. 41, pp. 1306-1319, 2006.

[9] R. Clavel, "Delta, a fast robot with parallel geometry," in *18th Int. Symp. on Industrial Robots*, Lausanne: IFS Publications, 1988, pp. 91-100.

[10] H.B. Choi, O. Company, F. Pierrot, A. Konno, T. Shibukawa, and M. Uchiyama, "Design and control of a novel 4-DOF parallel robot H4," in *Proc. IEEE Int. Conf. Robot. Auto.*, 2003, pp. 1185-1190.

[11] S. Krut, O. Company, M. Benoit, H. Ota, and F. Pierrot, "I4 : New parallel mechanism for Scara motions," in *Proc. IEEE Int. Conf. Robot. Auto.*, 2003, pp. 1875-1880.

[12] O. Company, F. Marquet, and F. Pierror, "A new high-speed 4-DOF parallel robot synthesis and modeling issues," *IEEE Trans. Robot. Auto.*, vol. 19, no. 3, pp. 411–420, June 2003.

[13] S. Krut, V. Nabat, O. Company, and F. Pierrot, "A high-speed parallel robot for Scara motions," in *Proc. IEEE Int. Conf. Robot. Auto*, 2004, pp. 4109-4115.

[14] O. Salgado, O. Altuzarra, V. Petuya, A. Hernández, "Synthesis and Design of a Novel 3T1R Fully-Parallel Manipulator," *J. Mech. Design*, vol. 130, no. 4, pp. 2008.

[15] G. Gogu, "Structural synthesis of fully-isotropic parallel robots with Schonflies motions via theory of linear transformations and evolutionary morphology," *Euro. J. Mechanics A/Solids*, vol. 26, pp. 242-269, 2007.

[16] S.M. Kim, W.K. Kim, and B.-J. Yi, "Kinematic analysis and optimal design of a 3T1R type parallel mechanism," in *Proc. IEEE Int. Conf. Robot. Auto.*, 2009, pp.2199-2204.

[17] J. Angeles and C.S. Lopez-Cajun, "Kinematic isotropy and the conditioning index of serial manipulators," *Int. J. Robot. Res.,* vol. 11, no. 6, pp. 560-571, 1992.

[18] L.J.Stocco, S.E.Salcudean and F. Sassani, "On the use of scaling matrices for task-specific robot design," *IEEE Trans. Robot. Auto*., vol. 15, no. 5, pp. 958-965, 1999.